Observations of Reduced Electron Gyroscale Fluctuations in National Spherical Torus Experiment *H*-Mode Plasmas with Large $E \times B$ Flow Shear

D. R. Smith,[1,*] S. M. Kaye,[1] W. Lee,[2] E. Mazzucato,[1] H. K. Park,[2] R. E. Bell,[1] C. W. Domier,[3] B. P. LeBlanc,[1]
F. M. Levinton,[4] N. C. Luhmann, Jr.,[3] J. E. Menard,[1] and H. Yuh[4]

[1]*Princeton Plasma Physics Laboratory, Princeton, New Jersey 08543, USA*
[2]*Pohang University of Science and Technology, Pohang 790-784, Korea*
[3]*Department of Applied Science, University of California at Davis, Davis, California 95616, USA*
[4]*Nova Photonics, Inc., Princeton, New Jersey 08540, USA*
(Received 27 January 2009; published 5 June 2009)

Electron gyroscale fluctuation measurements in National Spherical Torus Experiment *H*-mode plasmas with large toroidal rotation reveal fluctuations consistent with electron temperature gradient (ETG) turbulence. Large toroidal rotation in National Spherical Torus Experiment plasmas with neutral beam injection generates $E \times B$ flow shear rates comparable to ETG linear growth rates. Enhanced fluctuations occur when the electron temperature gradient is marginally stable with respect to the ETG linear critical gradient. Fluctuation amplitudes decrease when the $E \times B$ flow shear rate exceeds ETG linear growth rates. The observations indicate that $E \times B$ flow shear can be an effective suppression mechanism for ETG turbulence.

Anomalous electron thermal transport in magnetically confined plasma hinders efforts to achieve feasible magnetic fusion energy. In the past, transport models attributed anomalous transport to ion temperature gradient (ITG) and trapped electron mode (TEM) turbulence [1,2]. ITG and TEM turbulence are ion gyroscale instabilities with $k_\perp \rho_i \lesssim 1$, where $k_\perp$ is the fluctuation wave number perpendicular to the magnetic field and ρ_i is the ion gyroradius. Transport models based upon ITG/TEM turbulence were supported by observations of reduced ρ_i-scale fluctuations [3] in tokamak internal transport barriers (ITBs) [4,5]. When ITG/TEM transport models developed, $E \times B$ flow shear emerged as a universal suppression mechanism for plasma turbulence [6–9]. Indeed, observations of neoclassical ion thermal and particle transport in spherical torus (ST) *H*-mode plasmas with large toroidal rotation are consistent with $E \times B$ flow shear suppression of ITG/TEM turbulence [10,11]. As a rule of thumb, $E \times B$ flow shear reduces or suppresses ITG/TEM fluctuations when $\gamma_E \gtrsim \gamma$, where γ_E is the $E \times B$ flow shear rate and γ is the ITG/TEM linear growth rate.

Despite the success of ITG/TEM transport models with ion thermal and particle transport, the models cannot fully account for anomalous electron thermal transport observed in magnetically confined plasmas. Most notably, electron thermal transport remains anomalous in tokamak ITBs [12] and ST *H*-mode plasmas [10,11] despite neoclassical ion thermal and particle transport. The observations suggest that a mechanism beyond the ITG/TEM model can drive electron thermal transport. Recent nonlinear gyrokinetic simulations predict that electron temperature gradient (ETG) turbulence can produce experimentally relevant electron thermal transport for plasma regimes with mag-

netic shear $\hat{s} \gtrsim 0.4$ [13–17]. In addition, gyrokinetic simulations predict that ETG-driven electron thermal transport correlates with the formation of ETG radial streamers [13,14,16]. ETG turbulence occurs on the electron gyroscale with $k_\perp \rho_e \lesssim 1$, where ρ_e is the electron gyroradius. ETG and ITG modes are isomorphic in linear, electrostatic limits. For a deuterium plasma with temperatures $T_e = T_i$ and temperature scale lengths $L_{Te} = L_{Ti}$, ETG and ITG growth rates satisfy $\gamma_{\mathrm{ETG}} \sim 60\gamma_{\mathrm{ITG}}$, and mixing length estimates for ETG and ITG thermal diffusivities give $\chi_e^{\mathrm{ETG}} \sim \chi_i^{\mathrm{ITG}}/60$. Early transport models disregarded ETG turbulence because $\chi_e^{\mathrm{ETG}} \ll \chi_i^{\mathrm{ITG}}$. Recent nonlinear gyrokinetic simulations, however, point to substantial differences between the nonlinear dynamics of ETG and ITG turbulence [13,14]. Specifically, ETG turbulence generates zonal flows inefficiently compared to ITG turbulence, and ETG turbulence can saturate at a higher normalized amplitude than ITG turbulence. Indeed, simulations indicate that ETG turbulence can generate $\chi_e/\chi_e^{\mathrm{ETG}} \lesssim 10$, whereas ITG turbulence is limited to $\chi_i/\chi_i^{\mathrm{ITG}} \lesssim 2$ [16]. Sufficient $E \times B$ flow shear could break up ETG radial streamers and reduce ETG-driven electron thermal transport, but suppression of ETG turbulence by $E \times B$ flow shear was generally considered infeasible because $\gamma_{\mathrm{ETG}} \gg \gamma_{\mathrm{ITG}}$ [18].

To investigate ETG turbulence, a collective scattering system was installed on the National Spherical Torus Experiment (NSTX) [19]. The system measures electron gyroscale fluctuations with $k_\perp \rho_e \lesssim 0.6$ and $k_\perp \lesssim 20 \text{ cm}^{-1}$ [20–22]. The radial resolution of measurements is $\Delta R \approx \pm 2$ cm, and the k-space resolution is $\Delta k \approx 1 \text{ cm}^{-1}$. The system employs a tangential scattering geometry that exploits the large toroidal curvature of NSTX to enhance spatial localization along the probe beam such

that $\Delta L \lesssim 15$ cm [23,24]. Fluctuation measurements in NSTX L-mode plasmas revealed electron gyroscale fluctuations consistent with ETG turbulence, and enhanced fluctuations occurred when the electron temperature gradient exceeded the ETG linear critical gradient [25]. In this Letter, we report observations of electron gyroscale fluctuations in NSTX H-mode plasmas with large toroidal rotation and, accordingly, large $E \times B$ flow shear rates. Enhanced fluctuations occur when the electron temperature gradient is marginally stable with respect to the ETG linear critical gradient, and fluctuation amplitudes decrease when the $E \times B$ shear rate exceeds the ETG linear growth rate. The observations indicate that $E \times B$ flow shear can be an effective suppression mechanism for ETG turbulence.

A deuterium H-mode discharge with 700 kA plasma current, 4 MW neutral beam heating, and 4.5 kG toroidal field is shown in Fig. 1. Multipoint Thomson scattering (MPTS) measurements provide electron density (n_e) and electron temperature (T_e) profiles [26], and charge-exchange recombination spectroscopy (CHERS) measurements provide the ion temperature (T_i), carbon impurity toroidal velocity (V_{Tc}), and carbon impurity density (n_c) profiles [27]. The Mirnov signal in Fig. 1 indicates that low-frequency MHD activity is steady-state for 300–450 ms, and the neutron signal indicates that disruptive events are absent for 230–500 ms. TRANSP [28,29] calcu-

lates the equilibrium $E \times B$ shear rate from MPTS and CHERS measurements and LRDFIT equilibrium reconstructions [30]. LRDFIT equilibria are constrained by pitch angle measurements from a motional stark effect diagnostic [31]. NCLASS calculations within TRANSP provide the toroidal and poloidal velocity (V_T and V_P, respectively) for the deuterium fuel ions, and the poloidal velocity is assumed to be neoclassical. Using calculated and derived quantities from TRANSP, the Hahm-Burrell formula provides the $E \times B$ shear rate. n_e uncertainties from MPTS and T_i, V_{Tc}, and n_c uncertainties from CHERS provide error bars for the $E \times B$ shear rate. The gray box at $R = 133 \pm 2$ cm in Fig. 1 marks the location of fluctuation measurements. Note that the measurement location is near the peak $E \times B$ shear in the core plasma. The magnetic shear $\hat{s} \equiv (r/q)(dq/dr)$ is calculated from LRDFIT equilibrium reconstructions. The $\hat{s}$ uncertainty is calculated using a standard q uncertainty $\delta(q) = 0.15$. The radial variation of $\hat{s}$ in the measurement region is greater than to the $\hat{s}$ uncertainty. The magnetic shear at the measurement location $\hat{s} \approx 1.5$ is in the range in which gyrokinetic simulations predict ETG turbulence can produce experimentally relevant electron thermal transport [15,16].

Fluctuation measurements at $R = 133 \pm 2$ cm and $r/a = 0.5$–0.6 are shown in Fig. 2. The measurements correspond to fluctuations with $k_\perp \rho_e \approx 0.17$–0.21 and $k_\perp \rho_s \approx 10$–12 ($\rho_s$ is the ion sound Larmor radius). Asymmetric spectral features in Fig. 2 are the fluctuations of interest, and spurious reflections from the probe beam produce the large signal at zero frequency [22,25]. The fluctuation amplitude initially decreases at 300 ms, with an amplitude minimum at about 425 ms, and then the fluc-
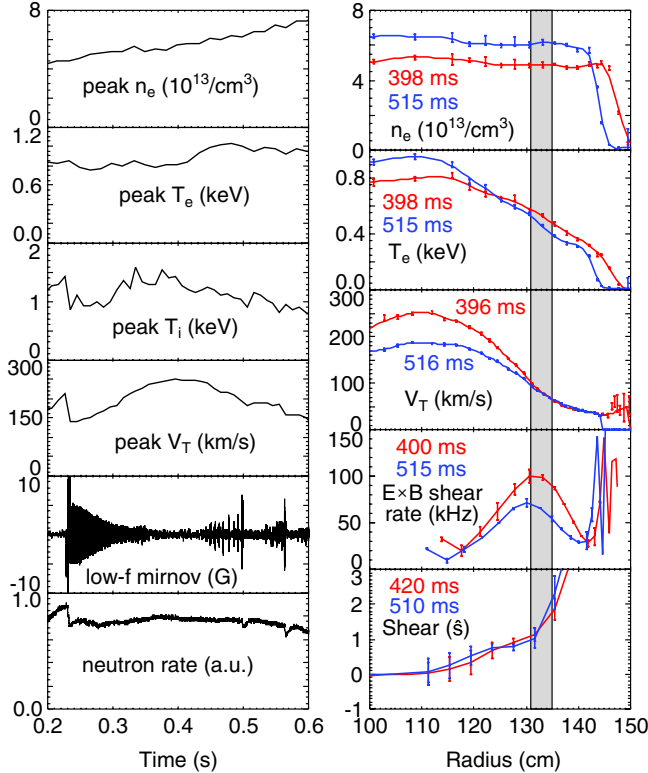
FIG. 1 (color online). Discharge 124 888 with fluctuation measurements at $R = 133 \pm 2$ cm and $r/a = 0.5$–0.6 (gray box).
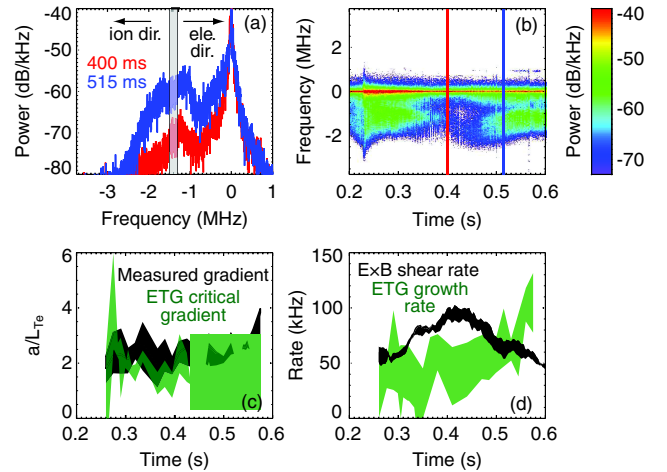
FIG. 2 (color online). Fluctuation measurements and linear gyrokinetic calculations for the discharge in Fig. 1 at $R = 133 \pm 2$ cm and $r/a = 0.5$–0.6. (a),(b) Fluctuation measurements with $k_\perp \rho_e \approx 0.17$–0.21. The gray box marks the Doppler shift from toroidal rotation. (c) Measured electron temperature gradient and ETG critical gradient and (d) ETG growth rate and $E \times B$ flow shear rate. The bands illustrate variations for $R = 133 \pm 2$ cm.

tuation amplitude increases. Positive frequency in Fig. 2 corresponds to fluctuations that propagate with a wave vector component in the electron diamagnetic direction in the *lab* frame. Toroidal rotation induces a Doppler shift of about 1.4 MHz toward the ion diamagnetic direction, so peak amplitudes in Fig. 2 correspond to fluctuations that propagate with a wave vector component in the electron diamagnetic direction in the *plasma* frame. The wave number range and propagation direction of measured fluctuations in Fig. 2 are consistent with ETG turbulence.

ETG modes are linearly unstable when the electron temperature gradient (a/L_{Te}) exceeds the ETG critical gradient. Linear gyrokinetic calculations with GS2 [14,32] provide the ETG growth rates and critical gradients shown in Fig. 2. The gradient and rate bands in Fig. 2 illustrate the radial variation for $R = 133 \pm 2$ cm. The uncertainty in the measured electron temperature gradient is about 20%, so the gradient uncertainty is comparable to the radial variation. Additional GS2 simulations indicate that the growth rate band is consistent with $\hat{s}$ and a/L_{Te} variations within the measurement region. The electron temperature gradient is near ETG marginal stability for 300–550 ms, so linear stability analysis cannot explain variations in fluctuation amplitudes. The $E \times B$ flow shear rate and ETG linear growth rate, however, show the necessary relationship to explain variations in the fluctuation amplitudes. Specifically, the growth rate initially exceeds the $E \times B$ shear rate, but the $E \times B$ shear rate surpasses the growth rate at about 380 ms. After about 470 ms, the $E \times B$ shear rate decreases to a level comparable to the growth rate. Minimum fluctuation amplitudes occur when the $E \times B$ shear rate exceeds the ETG growth rate, that is, during 380–470 ms. The observations indicate $E \times B$ flow shear can reduce the amplitude of ETG turbulence.

Similar observations occur at higher toroidal field. A deuterium *H*-mode discharge with 700 kA plasma current, 4 MW neutral beam heating, and 5.5 kG toroidal field is shown in Fig. 3. The Mirnov signal is steady-state during the period of interest, and the neutron signal indicates that disruptive events are absent. The gray box at $R = 133 \pm 2$ cm in Fig. 3 marks the location of fluctuation measurements. Again, the measurement location is near the peak $E \times B$ flow shear in the core plasma, and the local magnetic shear is in the range in which gyrokinetic simulations predict that ETG turbulence can produce experimentally relevant electron thermal transport.

Fluctuation measurements at $R = 133 \pm 2$ cm and $r/a = 0.5$–0.6 are shown in Fig. 4. The measurements correspond to fluctuations with $k_\perp \rho_e \approx 0.27$–$0.30$ and $k_\perp \rho_s \approx 16$–$18$. Again, peak amplitudes in Fig. 4 correspond to fluctuations that propagate with a wave vector component in the electron diamagnetic direction in the plasma frame. Enhanced fluctuations initially present at 400 ms decrease in amplitude later in time. Again, the gradient and rate bands in Fig. 4 illustrate the radial
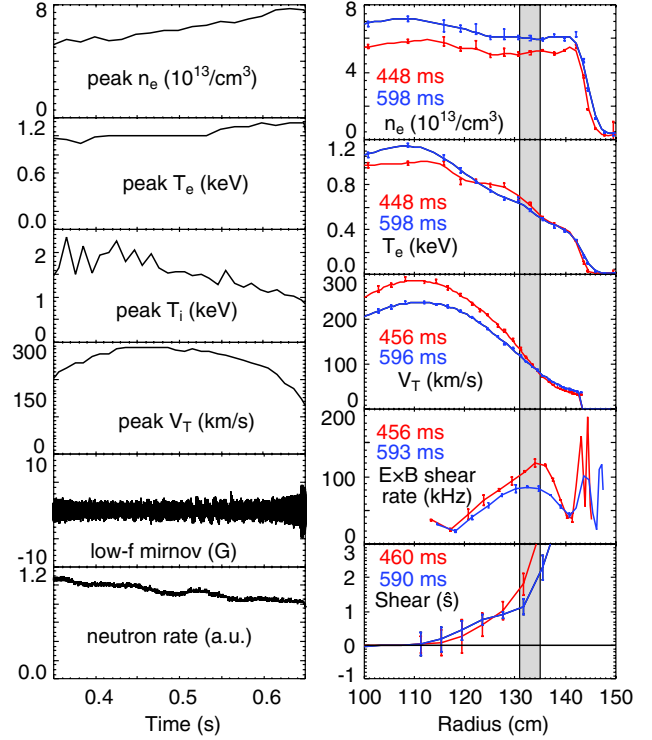
FIG. 3 (color online). Discharge 124 889 with fluctuation measurements at $R = 133 \pm 2$ cm and $r/a = 0.5$–0.6 (gray box).

variation for $R = 133 \pm 2$ cm, and the ETG growth rate band is consistent with $\hat{s}$ and a/L_{Te} variations within the measurement region. In addition, the decrease in growth rate for 500–600 ms is consistent with the decrease in $\hat{s}$ in the measurement region. The ETG mode is marginally
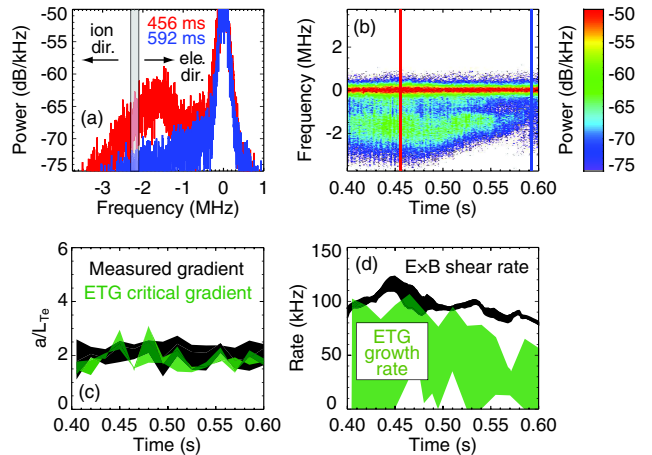
FIG. 4 (color online). Fluctuation measurements and linear gyrokinetic calculations for the discharge in Fig. 3 at $R = 133 \pm 2$ cm and $r/a = 0.5$–0.6. (a),(b) Fluctuation measurements with $k_\perp \rho_e \approx 0.27$–$0.30$. The gray box marks the Doppler shift from toroidal rotation. (c) Measured electron temperature gradient and ETG critical gradient and (d) ETG growth rate and $E \times B$ flow shear rate. The bands illustrate variations for $R = 133 \pm 2$ cm.

stable during the period of interest, so linear stability analysis cannot explain variations in fluctuation amplitudes. The ETG growth rate, however, decreases relative to the $E \times B$ shear rate as time progresses. Again, the observations indicate that $E \times B$ flow shear can reduce the amplitude of ETG turbulence.

Compared to Fig. 4, the observations in Fig. 2 show a clearer relationship among fluctuation amplitudes, ETG growth rates, and $E \times B$ shear rates. On the other hand, the electron temperature gradient in Fig. 4 tracks the ETG critical gradient closer than the electron temperature gradient in Fig. 2. Collectively, both observations indicate that $E \times B$ flow shear can reduce or suppress ETG turbulence. Finally, the measured electron temperature gradient does not exceed the ETG critical gradient by more than about 20% in the measurement region for both observations. Accordingly, the electron temperature profile may experience ''stiffness'' due to the ETG critical gradient.

In summary, electron gyroscale fluctuations measured in NSTX H-mode plasmas with large toroidal rotation are consistent with ETG turbulence. During times of interest, the electron temperature gradient is marginally stable with respect to the ETG linear critical gradient. Measurements reveal enhanced fluctuations with amplitudes that decrease when the equilibrium $E \times B$ shear rate exceeds the ETG linear growth rate. The observations indicate that $E \times B$ flow shear can be an effective suppression mechanism for ETG turbulence.

---

*Present address: Department of Engineering Physics, University of Wisconsin–Madison, Madison, WI 53706, USA.
drsmith@pppl.gov

[1] M. Kotschenreuther, W. Dorland, M. A. Beer, and G. W. Hammett, Phys. Plasmas **2**, 2381 (1995).
[2] R. E. Waltz *et al.*, Phys. Plasmas **4**, 2482 (1997).
[3] E. Mazzucato *et al.*, Phys. Rev. Lett. **77**, 3145 (1996).
[4] F. M. Levinton *et al.*, Phys. Rev. Lett. **75**, 4417 (1995).
[5] E. J. Strait *et al.*, Phys. Rev. Lett. **75**, 4421 (1995).
[6] K. H. Burrell, Phys. Plasmas **4**, 1499 (1997).
[7] E. J. Synakowski *et al.*, Phys. Rev. Lett. **78**, 2972 (1997).
[8] E. J. Synakowski *et al.*, Phys. Plasmas **4**, 1736 (1997).
[9] C. M. Greenfield *et al.*, Phys. Plasmas **4**, 1596 (1997).
[10] S. M. Kaye *et al.*, Nucl. Fusion **47**, 499 (2007).
[11] S. M. Kaye *et al.*, Phys. Rev. Lett. **98**, 175002 (2007).
[12] B. W. Stallard *et al.*, Phys. Plasmas **6**, 1978 (1999).
[13] W. Dorland, F. Jenko, M. Kotschenreuther, and B. N. Rogers, Phys. Rev. Lett. **85**, 5579 (2000).
[14] F. Jenko, W. Dorland, M. Kotschenreuther, and B. N. Rogers, Phys. Plasmas **7**, 1904 (2000).
[15] F. Jenko and W. Dorland, Phys. Rev. Lett. **89**, 225001 (2002).
[16] W. M. Nevins *et al.*, Phys. Plasmas **13**, 122306 (2006).
[17] R. E. Waltz, J. Candy, and M. Fahey, Phys. Plasmas **14**, 056116 (2007).
[18] E. J. Doyle *et al.*, Nucl. Fusion **47**, S18 (2007).
[19] M. Ono *et al.*, Nucl. Fusion **40**, 557 (2000).
[20] D. R. Smith *et al.*, Rev. Sci. Instrum. **75**, 3840 (2004).
[21] W. Lee *et al.*, Rev. Sci. Instrum. **79**, 10E723 (2008).
[22] D. R. Smith *et al.*, Rev. Sci. Instrum. **79**, 123501 (2008).
[23] E. Mazzucato, Phys. Plasmas **10**, 753 (2003).
[24] E. Mazzucato, Plasma Phys. Controlled Fusion **48**, 1749 (2006).
[25] E. Mazzucato *et al.*, Phys. Rev. Lett. **101**, 075001 (2008).
[26] B. P. LeBlanc *et al.*, Rev. Sci. Instrum. **74**, 1659 (2003).
[27] R. E. Bell, Rev. Sci. Instrum. **77**, 10E902 (2006).
[28] R. J. Hawryluk, in *Physics of Plasma Close to Thermonuclear Conditions* (Pergamon, New York, 1981).
[29] R. J. Goldston *et al.*, J. Comput. Phys. **43**, 61 (1981).
[30] J. E. Menard *et al.*, Phys. Rev. Lett. **97**, 095002 (2006).
[31] F. M. Levinton *et al.*, Phys. Plasmas **14**, 056119 (2007).
[32] M. Kotschenreuther, G. Rewoldt, and W. M. Tang, Comput. Phys. Commun. **88**, 128 (1995).